Catalysis Science & Technology



PAPER View Article Online View Journal



Cite this: DOI: 10.1039/d4cy01310g

Illustrating the surface chemistry of nitrogen oxides (NO_x) adsorbed on rutile TiO_2 (110) with the aid of STM and AIMD simulation†

S. Muthukrishnan, (Dab R. Vidya (Dab and Anja Olafsen Sjåstad (Dab and Anja Olafsen Sjästad (Dab anja

The family of nitrogen oxides such as NO, NO₂, and N₂O is considered as major anthropogenic environmental pollutants. Understanding the chemical interaction between adsorbed NO_x molecules and the rutile TiO_2 surface is important for environmental NO_x reduction. In this work, we have derived the adsorption mechanism of nitrogen oxide (NO_x) molecules on the rutile TiO_2 (110) surfaces by using density functional theory (DFT)-based computations. The most suitable adsorption sites for the nitrogen oxide molecules on the TiO_2 (110) surfaces are identified from the adsorption energetics. The complete charge flow process is understood for various NO_x adsorbed on the surface. The variation in the adsorption mechanism of NO, NO₂, and N₂O molecules was explored. *Ab Initio* Molecular Dynamics (AIMD) simulations are performed to study the stability of NO_x-adsorbed TiO_2 surfaces. Further insights on the ensuing modifications of the TiO_2 (110) surfaces, as well as their structural and thermodynamic stability, are derived. The Scanning Tunneling Microscope (STM) images of the rutile TiO_2 (110) surfaces and with the adsorbents are simulated for the first time, which helps to find the surface morphology of NO_x adsorbed on the TiO_2 surface. The influence of individual constituents of the adsorbed molecules and the surface is explored by analyzing the intricate features of their electronic structures. The present work provides guidelines exploring the interactions of NO_x pollutants adsorbed on rutile TiO_2 (110) surfaces.

Received 29th October 2024, Accepted 19th January 2025

DOI: 10.1039/d4cy01310g

rsc.li/catalysis

1. Introduction

The anthropogenic emission of nitrogen oxides produces adverse environmental effects, such as the destruction of stratospheric ozone, the greenhouse effect, and acid rain. The emission of nitrogen oxide affects the chemistry of the stratosphere, global radiation balance, and environmental nitrogen cycle. The concentration of nitrous oxide has continuously increased worldwide since the industrial revolution. The nitrogen oxide family comprises nitrogen monoxide (NO), nitrogen dioxide (NO₂), nitrous oxide (N₂O), and nitrogen pentoxide (N₂O₅) gases. Reducing these harmful pollutants through photocatalysts is considered the most promising approach. In the past, common transition metal oxides such as TiO_2 , CeO_2 , CuO, Cr_2O_3 , Fe_2O_3 , and SnO_2 are widely studied

For reducing the harmful NO_x content, studying the interaction between adsorbed molecules and oxide surfaces is necessary. The transition metal doping, such as Mn and Fe, enhances the NO_2 adsorption. From the literature, it is known that the particular site in the oxide surface is considered an active site for the adsorption of NO molecules. Previous studies investigated various surface termination and heterostructure models to uncover the interaction between adsorbed NO_x and the transition metal oxide surfaces, aiming to elucidate the NO_x molecular dissociation. 10,11

Using ${\rm TiO_2}$ as a photocatalyst to reduce the atmospheric ${\rm NO_x}$ content is considered to be a promising approach. ${\rm TiO_2}$ is known as a good semiconductor material with a bandgap of 3 to 3.2 eV and holds potential for photocatalytic degradation. ^{12,13} Its advantageous properties such as non-toxicity, chemical stability, thermal stability, photostability, and costeffectiveness thus make it widely useful as a photocatalyst in various industrial applications. ¹⁴ However, pure ${\rm TiO_2}$ exhibits photoactivity exclusively in the UV region of the solar spectrum. In our previous study, we demonstrated that introducing transition metal doping enhances photo-activity, enabling the absorption of visible light by reducing its bandgap. ¹⁵ Ramamoorthy *et al.* conducted a first principles study on the

because of their superior photocatalytic properties for reducing harmful pollutants.⁴⁻⁶

^a Centre for Materials Informatics (C-MaIn), Sir. C.V. Raman Science Block, Anna University, Sardar Patel Road, Guindy, Chennai 600025, India. E-mail: vidyar@annauniv.edu

b Computational Laboratory for Multifunctional Materials (CoLaMM), Department of Physics, Anna University, Sardar Patel Road, Guindy, Chennai 600025, India ^c Centre for Materials Science and Nanotechnology, Department of Chemistry, University of Oslo. PO Box 1033. Blindern. N-0315 Oslo. Norway

 $[\]dagger$ Electronic supplementary information (ESI) available. See DOI: ${\bf https://doi.org/10.1039/d4cy01310g}$

energetics of different stoichiometric rutile surfaces and revealed that rutile (110) surfaces possess lower surface energy compared to the (001) surface, which is attributed to their dangling bonds. Consequently, they concluded that among surfaces such as (110), (100), (011), and (001), rutile TiO₂ (110) is the most thermodynamically stable surface. 16,17 The rutile TiO2 (110) surface offered different adsorption sites for gas molecules, including five coordinated titanium sites (Ti_{5c}), three coordinated oxygen sites (O_{3c}), and two coordinated bridge oxygen sites (O2c), which will be illustrated in the following section. 18

Sorescu et al. explored the adsorption of NO molecules on TiO2 rutile (110) surfaces, highlighting the Ti5c site with Ti-NO configurations as the preferred site. 19 Several studies were carried out to improve the reduction of harmful NO_x under various reaction conditions. 12,20 N₂O molecule adsorption tends to favor the TiO2 surface with oxygen vacancies, and its dissociation occurs through reduction into N2.21 The surface morphology of the rutile TiO₂ (110) surface for the NO adsorption has been studied previously. Scanning Tunneling Microscopy (STM) is widely used to study the morphology of the surfaces.²² Point defects on TiO₂ nanoparticles facilitate NO2 detection, rendering the TiO2 surface more favorable for NO₂ adsorption.²³ Rutile TiO₂ (110) was also utilized to study the mechanism of the NO2 to HONO conversion with water molecules through an electronic structure study.²⁴ Mino et al. conducted both experimental and theoretical work on NO adsorption on the TiO2 surface and identified the preference for NO molecule adsorption with the N down configuration.²⁵ Previously, several attempts were made to explore the intrinsic characteristics of TiO2 for various energy and environmental applications. 26,27

To achieve the photocatalytic reduction of NO_x molecules, understanding the chemical interaction of the NO_x molecules with the oxide surface is crucial. Therefore, we conducted an extensive theoretical investigation aimed at comprehending the adsorption and charge transfer mechanism of various NO_x molecules such as NO, NO₂, and N₂O on different adsorption sites of the rutile TiO2 (110) surfaces. Our study encompassed the stoichiometric TiO2 rutile (110) surfaces to explore NO_x molecule adsorption possibilities. Employing the simulated STM allowed us to explain the surface electronic structure, molecule configuration, and orbital distribution on an atomic scale. It also aids our investigation into the orbital distribution of NO_x molecules on TiO₂ surfaces on the atomic scale.28

In addition, we utilize the Bader charge analysis and Projected Density of States (PDOS) analysis to examine the charge transfer dynamics between the surface and adsorbed molecules. Crystal Orbital Hamiltonian Population (COHP) analysis and charge density plots are employed to analyze the bonding characteristics between the adsorbed NO_x molecules and the TiO2 surface. Notably, before our study, there had been no investigation into the thermodynamic stability of NO_x molecules adsorbed on the TiO₂ (110) surface. To fill this gap, we employed Ab Initio Molecular Dynamics (AIMD) simulations at room temperature, presenting for the first time a comprehensive report on the thermodynamic stability of the adsorbed NO_x molecules on the TiO₂ surface.

2. Computational details

The density functional theory calculations are performed by plane-wave-based pseudopotential approximation, which is implemented in the Vienna Ab initio Simulation Package (VASP). 29,30 The generalized gradient approximation by the Perdew, Burke, and Ernzerhof (PBE) formalism was followed for the exchange-correlation functional.31,32 The kinetic energy cutoff of 500 eV is given for the expansion of the electron wave function through the plane wave basis set. For modeling the slabs, a vacuum of 15 Å is introduced along the Z-direction. In this work, a 3×1 supercell of the rutile TiO2 (110) surface with three layers of atoms was used. Except for the bottom-most layer of the surface, all the atoms are completely optimized with force and stress minimization. Since in our slab model the lattice parameter was a =8.87 Å and b = 6.49 Å, for convenience of structure convergence, a uniform 4 × 4 × 1 Monkhorst-Pack k-point mesh was used for Brillouin zone integration, as per the previous study.33 The convergence is reached by setting the threshold value as 10⁻⁶ eV and 0.01 eV Å⁻¹ for energy and force, respectively. The charges of the atoms on the surface and adsorbed molecules are calculated by Bader charge analysis.34 The van der Waals dispersion was included by the DFT-D3 method by Grimme.³⁵ The VESTA package was used for the visualization of the slab models.36 XcrySDen program was used for the visualization of charge density plots.³⁷ VASPKIT was used as a post-processing tool.³⁸ The chemical bonding between the adsorbed molecule and the surface was analyzed using COHP techniques as implemented in the LOBSTER package.³⁹ The ab initio molecular dynamics method, as implemented in the VASP code, was used to study the dynamic and thermal stability of the material.40,41

The rutile TiO2 phase has a tetragonal crystal structure with a space group of $P4_2/mnm$. In this work, we have used the slab model with three layers of atoms with a thickness of about 9 Å. The optimized surface has the lattice parameter of a = 8.87 Å and b = 6.49 Å. On the surface, it has the termination of alternate rows of Ti_{5c} atoms and Ti_{6c} atoms, which are separated by the alternate row of O_{3c} atoms. The Ti_{6c} atoms are covered by O2c atoms, which are known as the bridge oxygen atoms. After the relaxation, the Ti_{6c} and O_{3c} atoms on the top layer are shifted upwards by 0.24 Å, the Ti_{5c} atoms are shifted downwards by 0.07 Å, and the bridge oxygen atom is shifted upward by 0.11 Å. On the rutile TiO₂ (110) surface, the Ti_{6c} and Ti_{5c} atoms are shifted in opposite directions, resulting in the rumpling in the plane, in agreement with the previous studies. 42,43 On the top of the TiO2 surface (Fig. 1), Ti_{5c}, O_{3c}, and O_{2c} are considered the various possible adsorption sites for the adsorption of gas molecules. 44,45

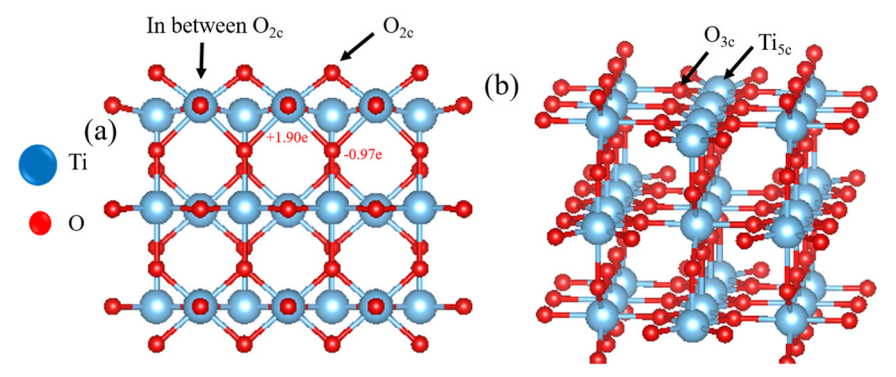


Fig. 1 The side view (a) and front view (b) of the optimized rutile TiO_2 (110) surface with different sites (Ti_{5c} , O_{3c} , and O_{2c}) for gas adsorption; the Ti and O atoms are represented in blue and red balls, respectively. The Bader charges for the pure rutile TiO_2 (110) surface are calculated as +1.90 e and -0.97 e for Ti and O, respectively.

3. Results and discussion

3.1. STM simulation of the TiO₂ rutile (110) surface and adsorption energy calculation

Scanning Tunneling Microscopy (STM) images usually provide a clear picture of the morphology of the surface by providing the direct real-space determination of the surface structure. Scanning Tunnelling Microscopy (STM) is used to study surfaces of materials and their adsorbed molecules to provide atomic-scale insights. It is also used to study the electronic structure of the surface and the orbital distribution of the adsorbed molecules. In the STM technique, a small

metal tip is brought so close to the surface that the vacuum tunneling resistance between the surface and tip becomes finite and measurable. As the tip scans the surface along two dimensions, a constant tunneling resistance is maintained by adjusting the height of the tip. In some cases, the tip is kept at a constant height while the biasing voltage is varied. In both cases, the contour map of the surface is generated.

$$I(r,V) \propto \int_{E_{\rm F}}^{E_{\rm F}+{\rm e}V} {\rm d}E \, n(r,E) \tag{1}$$

$$n(r, E) = \sum |\psi_{\mu}(r)|^2 \delta(\varepsilon_{\mu} - E)$$
 (2)

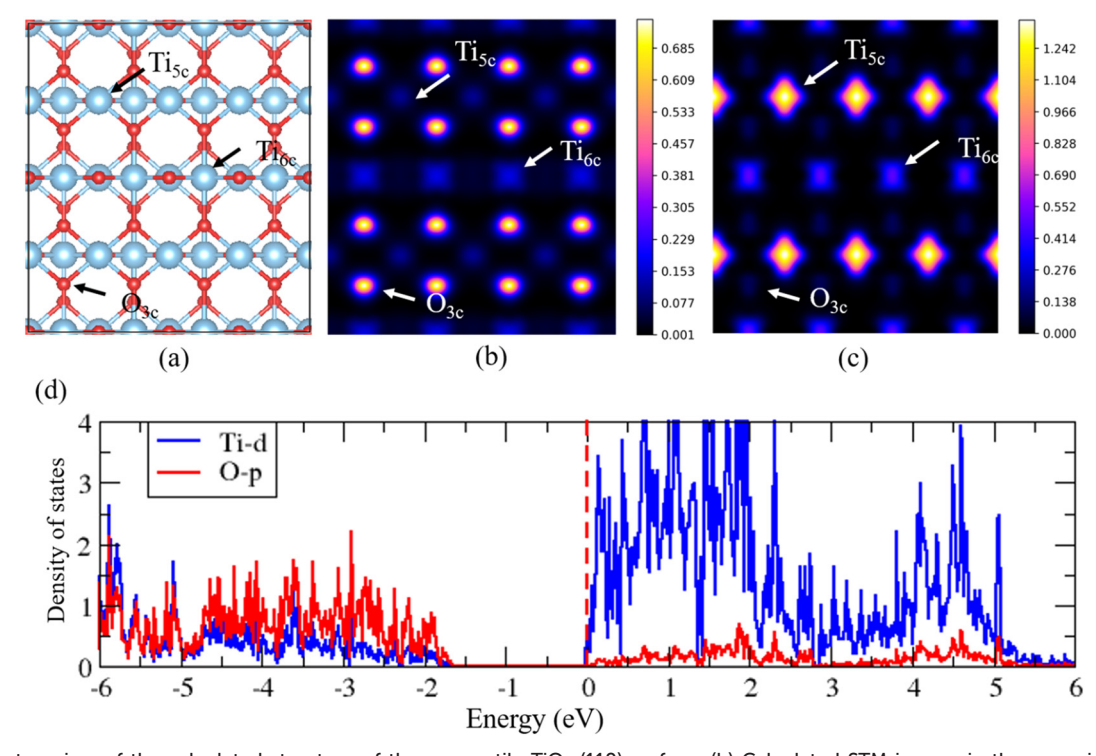


Fig. 2 (a) The top view of the calculated structure of the pure rutile TiO_2 (110) surface. (b) Calculated STM images in the occupied state of V = -2.0 V and (c) in the unoccupied state of V = 2.0 V. The Ti_{5c} , Ti_{6c} , and O_{3c} sites are indicated on the STM images. (d) Projected density of states (PDOS) for TiO_2 rutile (110).

The STM images can be obtained by the Tersoff-Hamann approximation, 48 which considers that the tunneling current I is dependent on the tip position r and the applied voltage V and proportional to the local density of states in the corresponding energy level (eqn (1)), where the local density of states is calculated from Kohn-Sham eigenvectors (ψ_{ij}) and eigenvalues (ε_{ij}) (eqn (2)). 49,50 The applied bias voltage is used to obtain the STM images in both occupied and unoccupied states.⁵¹

Fig. 2 shows the simulated STM images for the rutile TiO2 (110) surface at constant heights. The relaxed surface for pure rutile TiO2 (110) is shown in Fig. 2(a), which is terminated by Ti_{5c}, Ti_{6c}, O_{2c} and O_{3c} atoms. The simulated STM image for the occupied state with a bias potential of -2.0 V is shown in Fig. 2(b). In the occupied state, O_{3c} atoms are seen as bright spots, whereas Ti5c and Ti6c atoms are seen as dark spots. Since the STM images are the implication of the local density of states (LDOS), in the valence band, most of the states are from O 2p orbitals. In contrast, Ti 3d is the minority (see the projected density of states (PDOS) for pure rutile TiO2 (110) in Fig. 2(d)). This observation agrees well with the previous experimental and theoretical study.⁵² The simulated STM image for an unoccupied state with a bias potential of 2.0 V is shown in Fig. 2(c). Here, Ti_{5c} atoms are seen as bright spots (where we can observe the d-orbital distribution of Ti atoms), Ti_{6c} atoms as spots with less brightness as compared to Ti5c (since O_{2c} atoms covered the Ti_{6c} atoms), and the O_{3c} atoms are seen as dark spots. These features are related to Fig. 2(d); in the PDOS, in the conduction band, most of the states are from Ti 3d orbitals, whereas the O 2p states are very few. Since GGA functional underestimates the bandgap, we calculated PDOS using a more accurate hybrid functional (given in the ESI† Fig. S4). The calculated

bandgap is 3.2 eV, using HSE functional that slightly overestimated the bandgap.

The variation in the adsorption energy for different adsorption configurations for NO_x-adsorbed TiO₂ is plotted to understand the structural arrangement corresponding to the most preferred adsorption site (Fig. 3). The adsorption energy can be calculated using the following eqn (3):

$$E_{\rm ads} = E_{\rm NO_r/surface} - E_{\rm surface} - E_{\rm NO_r}$$
 (3)

where $E_{\rm ads}$ is the adsorption energy, $E_{\rm NO_s/surface}$ and $E_{\rm surface}$ represent the total energy of NO_x-adsorbed and pure rutile TiO₂ (110) surfaces, respectively, and E_{NO} is the total energy of isolated NO_x molecules. For the case of pure surfaces, among the various adsorption configurations, the NO molecule with an N down adsorption configuration on the O2c site, the NO2 molecule with an O down adsorption configuration on the Ti_{5c} site, and the N2O molecule with an N down adsorption configuration on the Ti_{5c} site of the TiO_2 surface are considered as the most stable (Table 1). The interaction of molecules with the surface can be further explained by various electronic structure analyses.

3.2. Adsorption of the NO molecule on the TiO2 rutile (110) surface

The rutile (110) surface has four adsorption sites: Ti_{5c}, Ti_{6c}, O_{2c}, and O_{3c} (Fig. 1). As the NO molecule has a linear structure, its adsorption on the rutile TiO2 (110) surface is modeled by bringing either the N atoms or O atoms downwards (Fig. 4 shows the NO adsorption with N-down and O-down configurations) on top of the above mentioned four adsorption sites. Among these eight different adsorption configurations, the NO molecule is found to have the highest

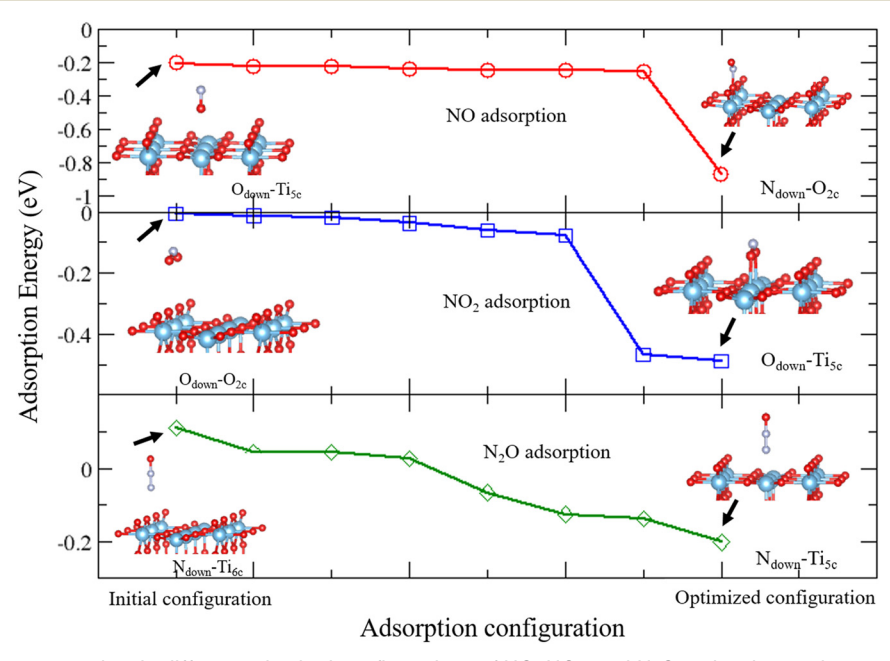


Fig. 3 Relative adsorption energy plots in different adsorbed configurations of NO, NO₂, and N₂O molecules on the pure rutile TiO₂ (110) surface.

Table 1 The calculated adsorption energy (eV) and bond length (Å) for NO, NO₂, and N₂O-adsorbed rutile TiO₂ (110) surfaces at different adsorption sites with N-down and O-down configurations

S. No.	Adsorption configuration	Adsorption of NO		Adsorption of NO ₂		Adsorption of N ₂ O		
		Adsorption energy (eV)	N-O bond length (Å)	Adsorption energy (eV)	N-O bond length (Å)	Adsorption energy (eV)	Bond length (Å)	
							N-O	N-N
1	(A) Top of Ti _{5c} (N down)	-0.2284	1.153	-0.0372	1.212	-0.2026	1.189	1.139
2	(B) In between the O _{2c} (N down)	-0.2441	1.149	-0.4676	1.214	0.1103	1.197	1.141
3	(C) Top of O _{3c} (N down)	-0.2589	1.147	-0.0767	1.210	-0.1262	1.188	1.142
4	(D) Top of O _{2c} (N down)	-0.8701	1.178	-0.0176	1.209	0.0261	1.200	1.142
5	(E) Top of Ti _{5c} (O down)	-0.2060	1.151	-0.4901	1.250	-0.0665	1.196	1.140
6	(F) In between the O _{2c} (O down)	-0.2506	1.147	-0.0128	1.210	0.0444	1.194	1.147
7	(G) Top of O _{3c} (O down)	-0.2481	1.150	-0.0593	1.212	-0.1392	1.204	1.140
8	(H) Top of O _{2c} (O down)	-0.2239	1.148	-0.0064	1.210	0.0438	1.197	1.140

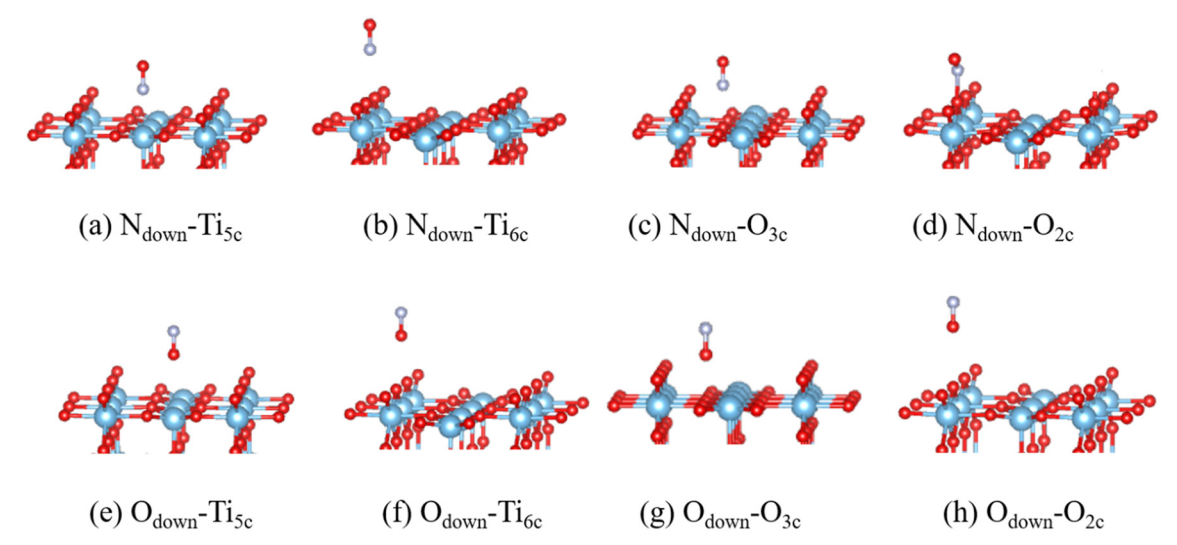


Fig. 4 The optimized geometries of the NO molecule adsorbed on different possible adsorption sites with both N down and O down configurations on the rutile TiO_2 (110) surface. The Ti, O, and N atoms are shown in blue, red, and white balls, respectively.

adsorption energy of about -0.87 eV on the O_{2c} site with an N-down configuration (Fig. 4(d)). As the N-down is attracted towards the O_{2c} site on the surface, the bond length of the NO molecule is slightly increased from 1.16 Å to 1.17 Å.

The analysis of the electronic structure and related parameters provides further insights into adsorption. The valence band (VB) of the TiO₂ surface is composed of hybridized Ti 3d and O 2p orbitals with a dominant presence of O 2p states. The unoccupied Ti 3d levels are predominant in the conduction band minimum (CBM). The isolated NO molecule has the characteristic of discrete, localized energy levels corresponding to the N-O molecular orbitals. These molecular orbitals are completely hybridized, and predominantly present between -9 and -7 eV in the VB and separated by an energy gap of 7 eV from the unoccupied energy states. It is interesting to note that the electronic structure of NO adsorbed on the rutile TiO₂ (110) surface undergoes significant modifications. As the NO molecules interact with the TiO₂ surface, the degeneracy between the N 2p and O 2p orbitals of the NO molecule is lifted as the N-atom moves closer to the surface,

thus elongating the N–O bond by 0.01 Å. For the isolated NO molecule, N 2p and O 2p states are falling on the Fermi level, indicating their partial occupancy. However, upon the adsorption on the ${\rm TiO_2}$ surface, these states move away from the Fermi level in the VB and CB.

While the DOS illustrates the presence of different energy states, the projected crystal orbital Hamiltonian population (pCOHP) indicates the nature of bonding to energy states. For instance, a positive pCOHP indicates the bonding states and a negative pCOHP indicates the anti-bonding states. ⁵³ A combined analysis in Fig. 5(a) and (b) illustrates that the predominant bonding states are present between -1 and -2 eV arising from N 2p, O(N) 2p, and O(Ti) 3d states. These states have nonnegligible bonding from -2 to -6 eV also. This implies that the N atom of the NO molecule forms a bonding interaction with the O atom of the TiO₂ surface. Hence, it is concluded that NO adsorption on the TiO₂ surface is chemisorption.

The charge density and charge transfer isosurface plots (Fig. 5(e) and (c)) enable us to visualize the actual bonding situation in the studied system. As discussed earlier, the N

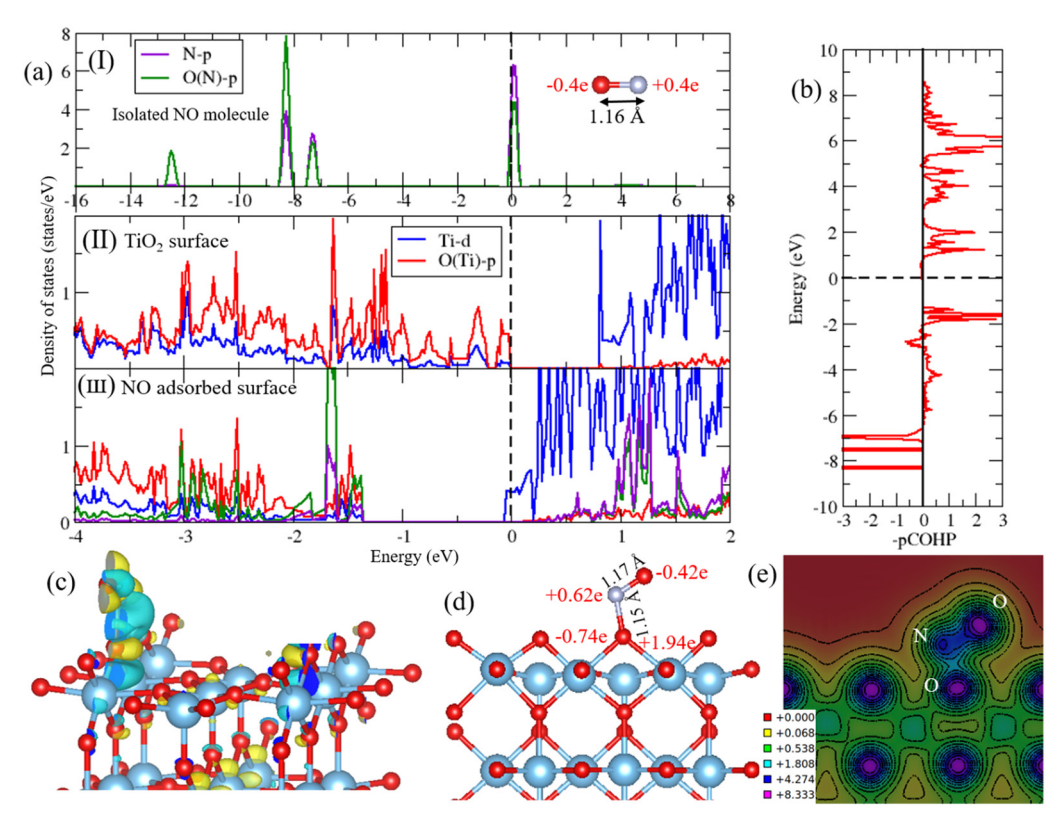


Fig. 5 Projected density of states (a) for the NO molecule adsorbed on the rutile TiO₂ (110) surface; the Fermi level kept at 0 eV, Bader charges, and bond length of isolated NO molecules are shown in the insets. COHP plots (b) for the $O_{(Ti)}$ -N bonding. Charge density difference plots (c) for NO adsorbed on the O_{2c} site with an isovalue of 0.003 e Å⁻³; here, yellow and blue contours represent the charge accumulation and depletion regions, respectively. Bader charges and bond lengths (d) for the NO adsorbed surface, and the charge density plot (e) for the NO adsorbed surface.

atom of NO comes closer to the TiO2 surface, thus sharing the electron with the O atom of the TiO2. More contours are seen between N and O(Ti) than between N and O(N) in Fig. 5(e), which emphasizes covalent bonding. The charge density transfer plot with an isovalue of 0.003 e Å⁻³ indicates charge accumulation and depletion by the yellow and light blue color isosurfaces, respectively. The light blue color isosurface seen between the N and O(Ti) atoms indicates the transfer of electrons from the N to O(Ti). The Bader charge calculation helps us to quantify the amount of charge transfer. In the pure TiO₂ (110) surface, the Bader charges on Ti and O atoms are +1.90e and -0.97e, respectively. They are the same for the isolated NO molecule, which are +0.40e and -0.40e for N and O atoms, respectively. Upon the NO adsorption on the TiO2 surface, the charge transfer scenario undergoes significant changes. The Ti and O atoms have +1.94e and -0.74e, respectively, whereas the N and O(N) atoms have +0.62e and -0.42e, respectively (Fig. 5(d)). As a result, the NO molecule gains a net charge of +0.20e from the surface. Hence, the surface gains electrons from the molecules. This can be seen from the PDOS, where CBM comes closer to the Fermi level (Fig. 5(aIII)). The noticeable changes in the Bader charges of N and O(Ti) further reinforce the transfer of charges between N and O(Ti) atoms.

The STM simulation helps to find the adsorbed configuration and geometry of the NO molecule on the rutile TiO₂

(110) surface.⁵⁴ The calculated STM images for NO adsorbed on the O_{2c} site of the rutile TiO₂ (110) surface are shown in Fig. 6. Fig. 6(a) shows the top view of the calculated geometrical structure of the rutile TiO2 (110) surface, where the NO molecule is adsorbed on the O2c site of the surface, with the N atom closer to the surface. Fig. 6(b) shows the simulated STM images for the occupied state with a bias voltage of -2.0 V; here, O(N) appears as bright spots and N appears as dull dark spots. The p orbital distributions reveal O_{3c} and a minute spot of Ti_{5c} was observed. Fig. 6(c) shows the simulated STM for an unoccupied state with a bias voltage of 2.0 V, where the O(N) appears as bright yellow spots, and N appears as dark blue spots, which clearly conveys that our results are in agreement with the previous study. 22 The Ti_{5c} and O_{3c} appear as less bright and less dark spots, respectively, where the p-orbital distribution of O_{3c} can also be seen from the STM images. From the bias-dependent simulated STM images of the NOadsorbed TiO2 surface, we can visualize the adsorbed configuration of the NO molecule on the O2c site of the surface, as well as the orbital distribution of the surface O atoms. Our calculated STM images are able to aid researchers in correlating the actual STM images for NOadsorbed TiO2 surfaces.

To study the thermal and dynamic stability of the NO adsorbed on the rutile TiO₂ (110) surface, Ab Initio Molecular

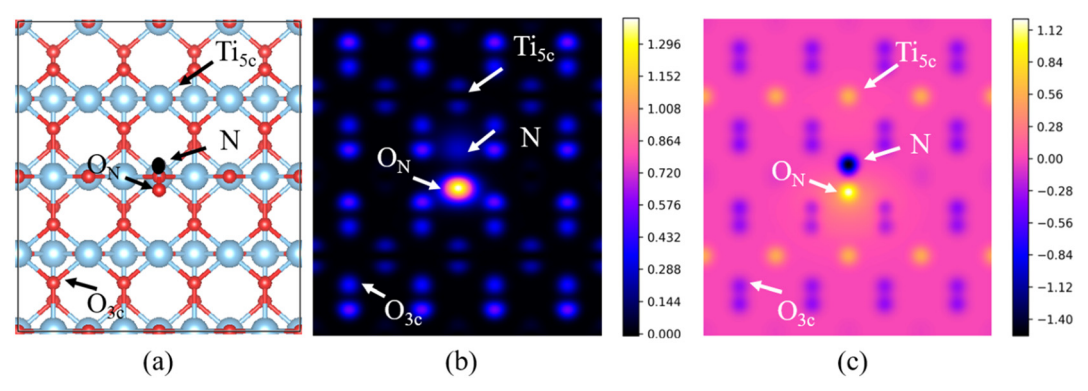


Fig. 6 (a) Top view of the optimized geometrical structure for NO adsorbed on the O_{2c} site of the rutile TiO₂ (110) surface; the Ti, O, and N atoms are shown in blue, red, and black balls, respectively. (b) Simulated STM image in the occupied state with V = -2.0 V. (c) Simulated STM image in unoccupied states with V = 2.0 V.

Dynamics (AIMD) simulation was performed. AIMD simulation is based on finding the electronic ground state and Hellmann-Feynman forces to each molecular dynamic step. The conjugate gradient algorithm is used to attain the energy minimization, and the wave function is predicted at each ionic step. 40 The thermal stability was analyzed by setting the starting temperature to 300 K for the AIMD simulation. Fig. 7(a) shows the temperature vs. time (fs) plots for 4000 steps for 1 fs. From the plots, it is found that the adsorbed surface remains thermally stable throughout the considered time steps. Fig. 7(b) shows the total energy vs. time step (fs), where the total energy fluctuates from -468 eV to -473 eV for the first 1000 fs. The fluctuation is less, and it remains stable at around -472 eV. At this energy range and time, considerable deformation in the adsorption configuration of the NO molecule on the TiO₂ surface occurs. Fig. 7(c) shows the initial and most stable (at 2081 fs) adsorbed configuration of the NO molecule on the O_{2c} site with the N down configuration. The bond length of NO is changed from 1.15 Å to 1.21 Å, and its distance from the top of the TiO₂ surface increases

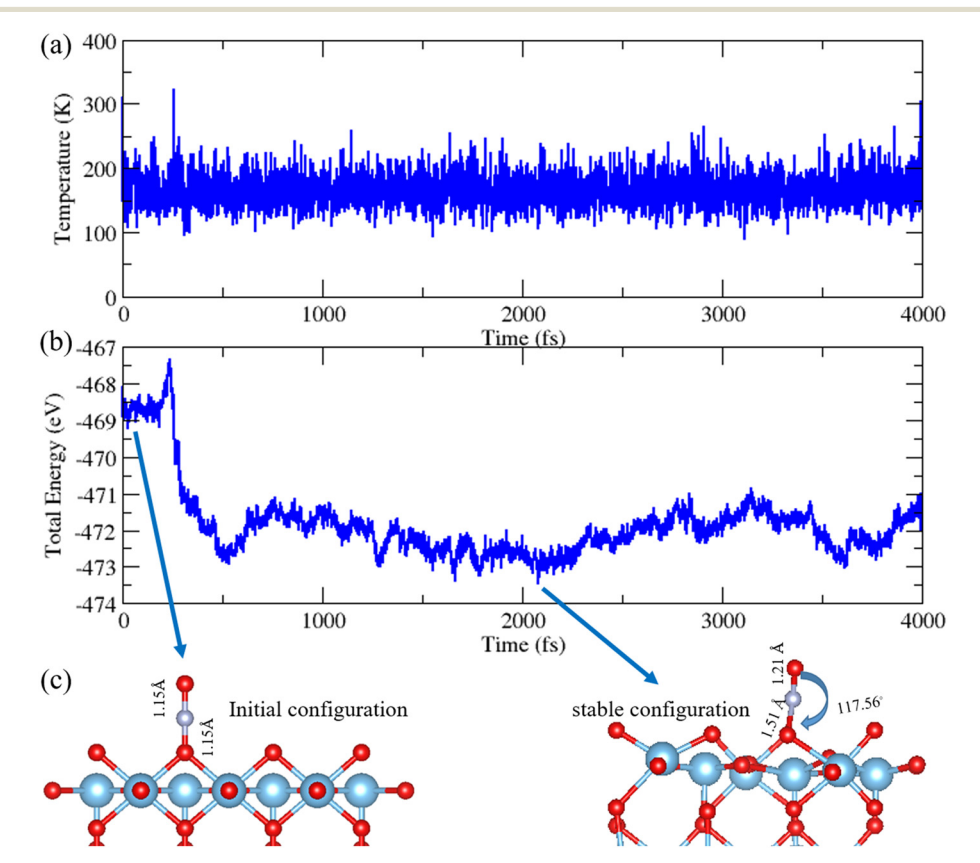


Fig. 7 Ab initio molecular dynamics simulations for NO adsorbed on the O_{2c} site of the rutile TiO₂ (110) surface. (a) Temperature vs. time step, (b) total energy vs. time step, and (c) the initial and stable configurations of the NO-adsorbed TiO2 surface.

from 1.15 Å to 1.51 Å in its stable final configuration. The NO molecule is slightly tilted, and it has an angle of 117.56° with the O_{2c} atom of the TiO₂ surface. It was understood that the bond length of the NO molecule and its distance from the surface are greater for a lower total energy range, and they are reversed for a higher total energy range. Hence, the NO molecule prefers to have an elongated bond length and a higher distance from the surface (see Fig. S5 in the ESI†).

3.3. Adsorption of NO2 on the TiO2 rutile (110) surface

The NO₂ molecule adsorption on the TiO₂ surface is modeled by N-down and O-down configurations (as shown in Fig. 8). Among these eight different adsorption configurations, the NO₂ molecule is found to have the highest adsorption energy of about -0.49 eV on the Ti_{5c} site with an O-down configuration (Fig. 8(e)). As the O atoms of the NO₂ molecule are attracted towards the Ti_{5c} site on the surface, the bond length of the NO₂ is increased from 1.21 Å to 1.25 Å, and the bond angle is reduced from 133.44° to 122.50°.

The isolated NO2 molecule has discrete, localized energy levels contributed by N and O p-orbitals in the energy range of -2 to -9 eV in the VB (Fig. 9(a)). Significant quantities of N 2p and O 2p orbitals of the NO2 molecule hybridize and fall at the Fermi level. The partial occupancy of the NO₂ molecular orbitals can be inferred from the peak of the DOS at the $E_{\rm F}$. After NO₂ is adsorbed on the TiO₂ surface, there are significant changes in its electronic structure. As the NO2 molecule interacts with the TiO2 surface, the O atoms of the NO2 come closer to the Ti atom of the surface thus elongating the N-O bond length by 0.04 Å. As the NO₂ molecule is adsorbed on the TiO2 surface, the N 2p and O 2p orbitals of the NO2 molecules are hybridized with O(Ti) 2p of the surface, depicted by the DOS in the energy range of 0 to -3 eV. The partially filled molecular level of NO2 becomes filled by gaining the electrons from the TiO2 surface. This fact is inferred from the DOS of N, O(1), and O(2) of the NO2 molecule (see Fig. S2 in the ESI†). The discrete peaks of O 2p DOS seen from -2 to -4 eV of the isolated NO2 molecule now become bonding states by hybridizing with the Ti 3d states in the -1.5 to -3 eV range. Therefore, a significant distinction is made between the bonding and anti-bonding states of NO2. The presence of N and O states within the Fermi level also implies improved stability of the configurations.

Further interactions of NO2 molecules with the TiO2 surface are discussed below. The charge density transfer isosurface plots are shown in Fig. 9(b). The Bader charges for isolated NO₂ molecules are -0.33e and +0.66e for O and N atoms, respectively, and after become -0.50e and +0.66e, respectively. This implies that the NO2 molecule gains a net negative charge of -0.34e from the rutile (110) surface (Fig. 9(c)). The higher interaction of NO2 on the surface shows that NO2 adsorption on the TiO₂ surface is chemisorption.

The simulated STM images for the NO2 adsorbed on the Ti_{5c} site of the rutile TiO₂ (110) surface are shown in Fig. 10. Here, in the occupied state (Fig. 10(b)), Ti_{5c} is seen as a dark spot, and O_{2c} and O_{3c} are seen as moderate bright spots. For the adsorbed NO2 molecule, the N atom is seen as a dark spot, and O(N) atoms are seen as bright spots. For the unoccupied state (Fig. 10(c)), the Ti_{5c} and O_{2c} are seen as dark spots and the O_{3c} is seen as bright spots with the p-orbital distribution. The adsorbed NO2 molecule can be identified by strong bright charge clouds on the surface; here, the N is seen as a bright spot, and $O_{(N)}$ is seen as a dark spot.

The thermal and dynamic stability of the NO₂-adsorbed TiO2 surface is further studied by ab initio molecular dynamics simulations. At the beginning of the AIMD simulation, the NO2 is symmetric with an equal O-N-O bond length of 1.24 Å, and a bond angle of 134.76°, and placed at a height of 2.32 Å from the surface. However, there is a significant

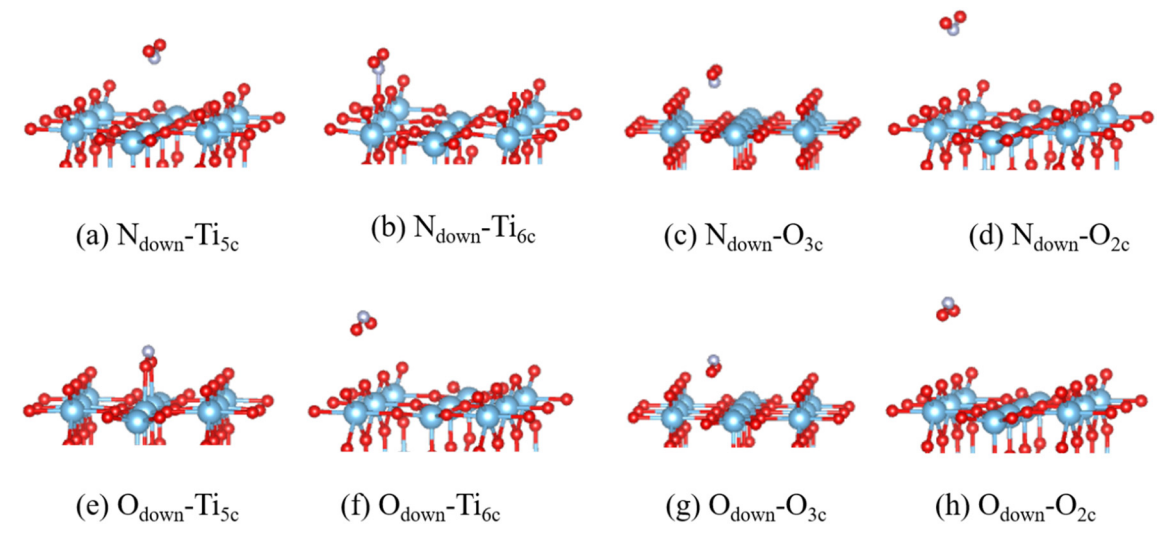


Fig. 8 The optimized geometries of the NO₂ molecule adsorbed on different possible sites with both N down and O down configurations on the rutile TiO₂ (110) surface. The Ti, O, and N atoms are shown as blue, red, and white balls, respectively.

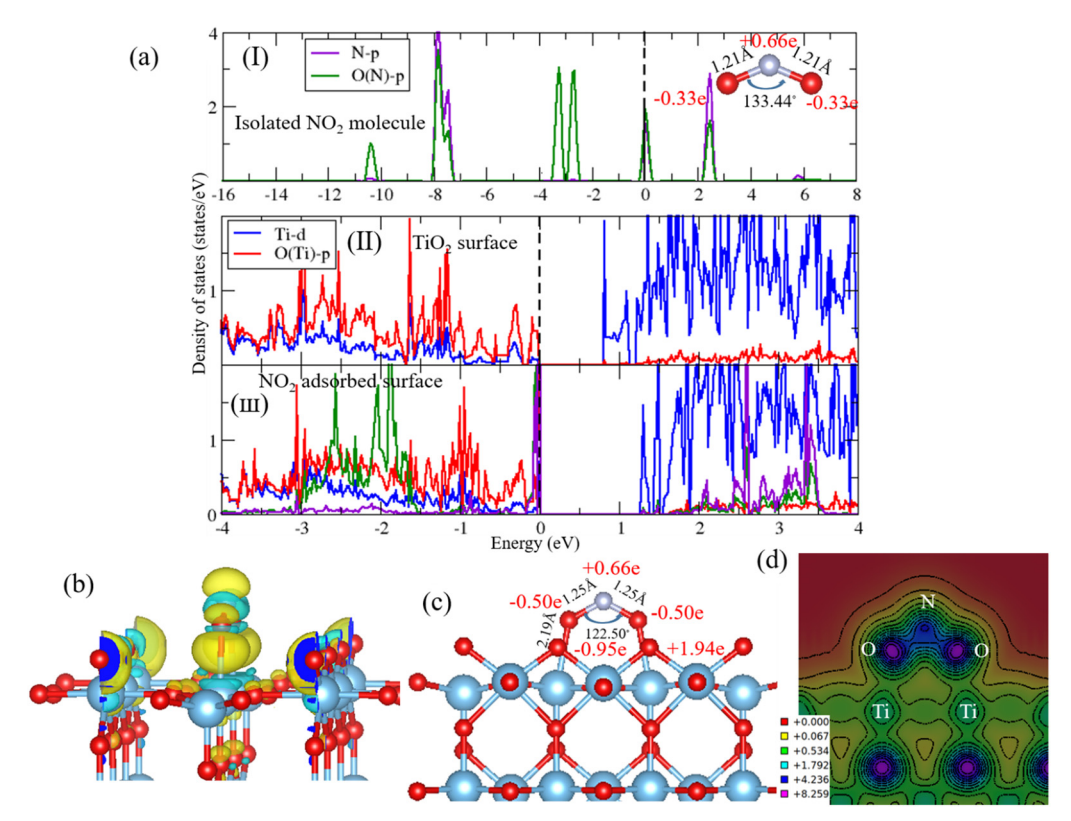


Fig. 9 Projected density of states plots (a) for the NO₂ molecule adsorbed on the rutile TiO₂ (110) surface; the Fermi level is fixed to 0 eV; the bond length and Bader charges of isolated NO₂ are shown in the inset. Charge density difference plots (b) for NO₂ adsorbed on the Ti_{5c} site with an isovalue of 0.003 e Å⁻³; here, yellow and blue contours represent the charge accumulation and depletion regions, respectively. (c) Bader charges and bond lengths of the NO2-adsorbed surface. (d) Charge density plot of the NO2-adsorbed surface.

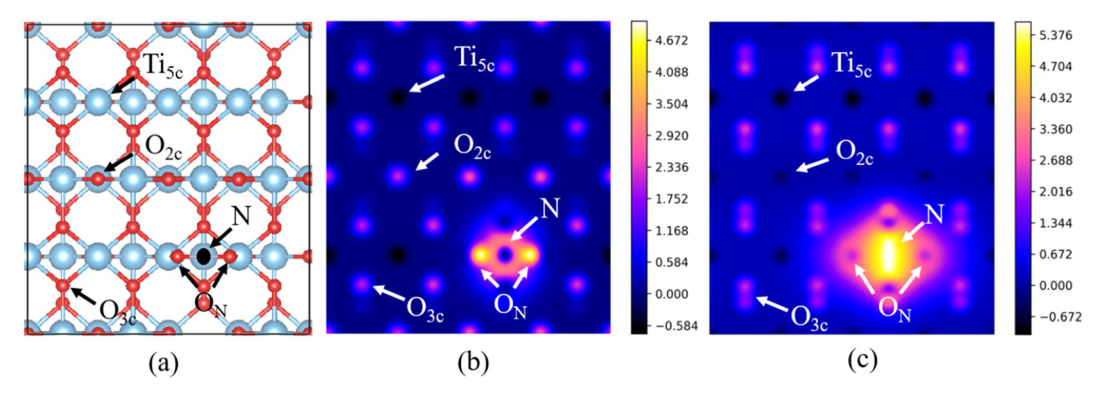


Fig. 10 (a) Top view of the calculated geometrical structure for NO₂ adsorbed on the Ti_{5c} site of the rutile TiO₂ (110) surface with the O-down configuration; the Ti, O, and N atoms are shown in blue, red, and black balls, respectively. (b) Simulated STM image of the occupied state with bias voltage V = -2.0 V. (c) Simulated STM image of unoccupied states with V = 2.0 V.

modification in the molecular structure with O-N-O bonds varying from 1.16 Å and 1.41 Å, and the bond angle is decreased to 112. 22°. Moreover, the molecule becomes tilted with distances of 1.77 Å to 2.01 Å from the surface. Because of this, the TiO2 (110) surface is also significantly affected, and the Ti-O6 octahedron is heavily distorted with an unequal bond length (Fig. 11(c)). Therefore, the initial configuration with symmetric molecular adsorption is the most preferred one which has the lower total energy.

3.4. Adsorption of N₂O on the TiO₂ rutile (110) surface

Similar to the previous cases, N₂O adsorption on the TiO₂ (110) surface is modeled with N-down and O-down configurations as the N2O molecule has a linear structure. Among the various adsorption sites, Ti_{5c} with N-down (Fig. 12(a)) has the highest adsorption energy of about -0.20 eV. In the previous cases, N2O adsorption on the TiO2 surface leads to the reduction in its N-O and N-N bond length by 0.01 Å.

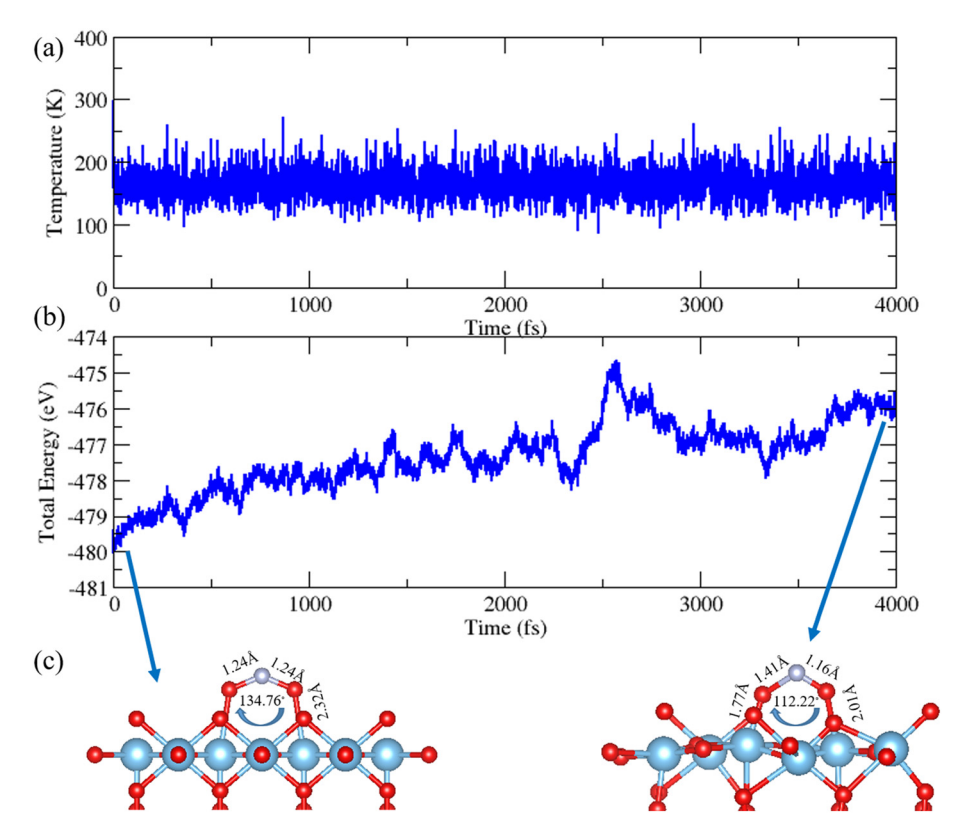


Fig. 11 Ab initio molecular dynamics simulations for NO₂ adsorbed on the Ti_{5c} site of the rutile TiO₂ (110) surface. (a) The temperature vs. time step (fs) plot for the NO2 molecule-adsorbed surface at 300 K for 4000 fs with a time step of 1 fs, which shows that the adsorbed surface is thermally stable throughout the 4000 fs time step. (b) The total energy vs. time step (fs) plot for the NO2 adsorbed surface. The total energy of the system increases constantly from -480 eV to -476 eV. (c) The initial and final adsorbed configurations of the NO₂ molecule.

An isolated N2O molecule has discrete energy states in the range of 0 to -7 eV in the VB (Fig. 13(a)). These states close to the Fermi level result from the hybridized N 2p and O 2p orbitals, respectively. After the adsorption of N2O, the bond lengths of N-O and N-N decreased to 1.18 Å and 1.13 Å, and the N 2p and O 2p states of N₂O shifted down in the VB, and became predominant in the range of -2 to -3.5 eV. They hybridize with the Ti 3d orbitals of the TiO2 surface also. The

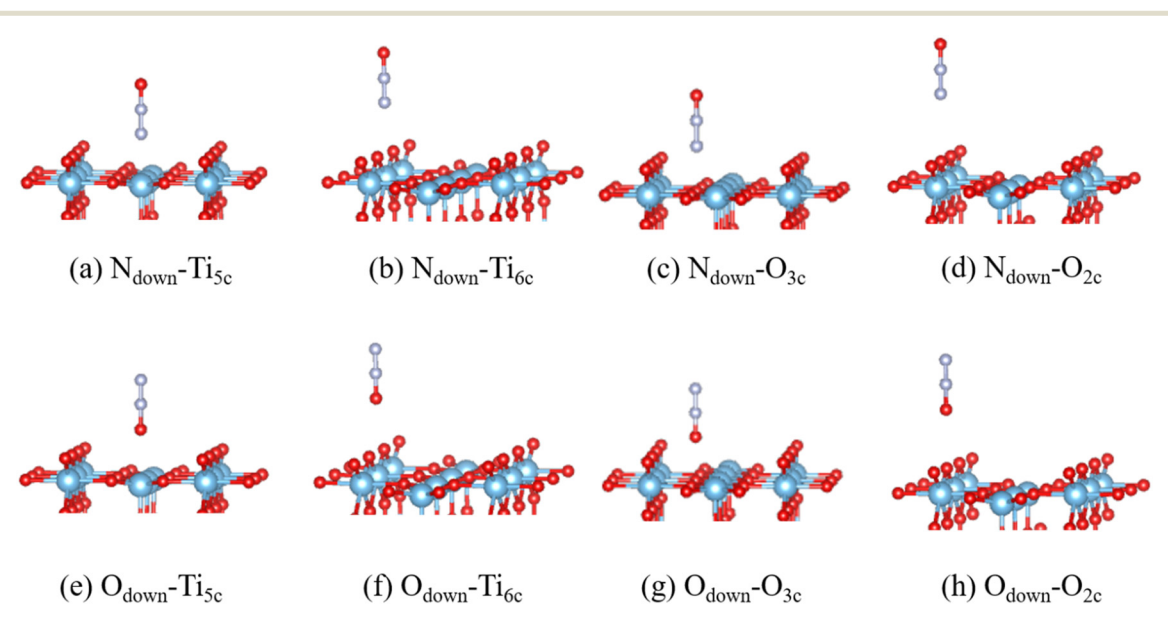


Fig. 12 The optimized geometries of the N₂O molecule adsorbed on different possible adsorption sites with both N down and O down configurations on rutile TiO₂ (110). The Ti, O, and N atoms are represented as blue, red, and white balls, respectively.

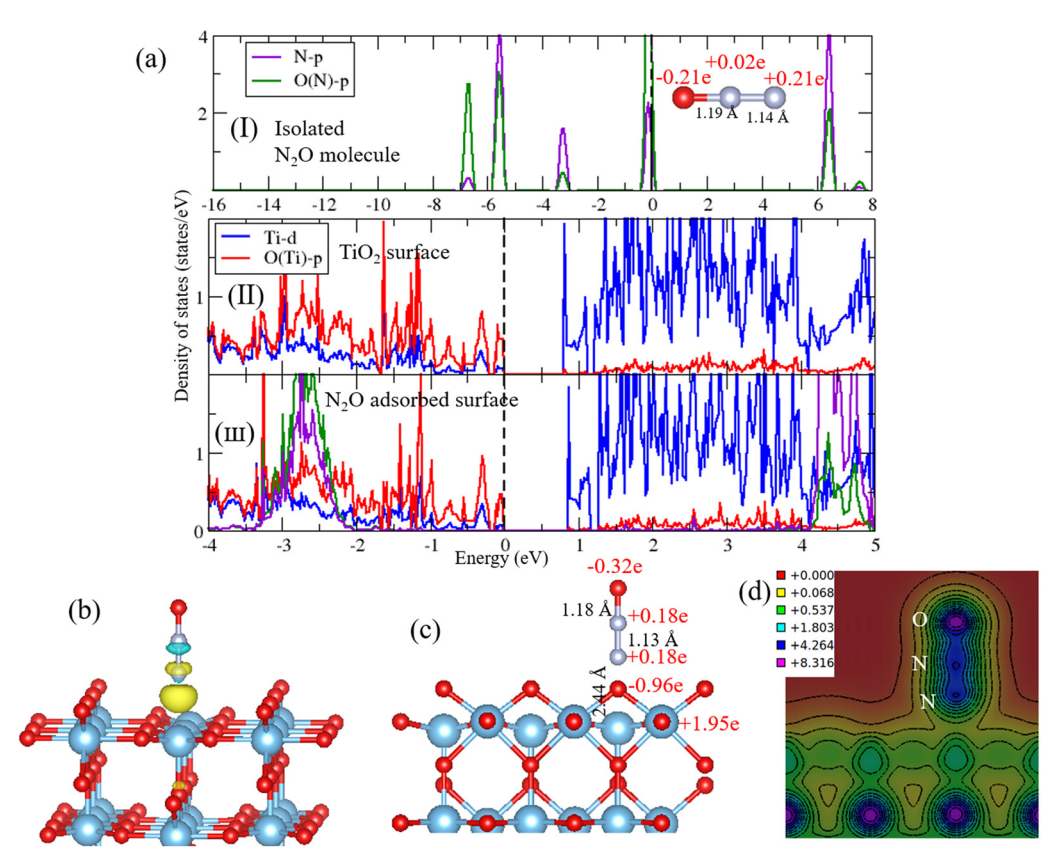


Fig. 13 Projected density of states plots (a) for the N_2O molecule adsorbed on the rutile TiO_2 (110) surface; the Fermi level was shifted to 0 eV; the Bader charges and bond length of the isolated N_2O molecule is shown in the inset. Charge density difference plot (b) for N_2O adsorbed on the Ti_{5c} site with an isovalue of 0.003 e Å⁻³, where yellow and blue contours represent the charge accumulation and depletion regions, respectively. (c) Bader charges and bond lengths of the N_2O -adsorbed surface. Charge density plot (d) of the N_2O adsorbed surface.

atom-wise PDOS plot is shown in Fig. S3 in the ESI.† The nitrogen atom close to the surface has lower states in the VB, whereas the one further away has unoccupied states.

The charge density difference plot for the N_2O adsorbed surface is shown in Fig. 13(b). It is observed that there are only a few charge accumulations and depletions between the N_2O and TiO_2 surfaces. The isolated N_2O molecule has Bader charges of -0.21e and +0.21e for O and N atoms, respectively, whereas the middle N atom has only +0.02e. After the adsorption, the charges on both N atoms become +0.18e, and that on the O atom is -0.32e (Fig. 13(c)). Hence, it is concluded that N_2O adsorption leads to significant charge redistribution in the molecule itself. Overall, N_2O molecules obtained a net charge of +0.04e from the surface. Here, the N_2O molecule provides the electrons to the TiO_2 (110) surface. The poor charge transfer and the least interaction of N_2O on the surface shows that N_2O adsorption on the TiO_2 surface is physisorption.

Fig. 14 shows the simulated STM images for N_2O adsorbed on the Ti_{5c} site on the rutile TiO_2 (110) surface. In the occupied state (Fig. 14(b)), Ti_{5c} is seen as dark spots, and O_{2c} and O_{3c} are seen as bright spots. The adsorbed N_2O can be identified by dark and less bright $O_{(N)}$ and N atoms, respectively. Fig. 14(c) shows the simulated STM image for an unoccupied state with a bias voltage of 2.0 V; here, the Ti_{5c} and O_{3c} are

seen as dark and bright spots, respectively. The adsorbed configurations of the N_2O molecule can be identified with strong bright charge clouds. In both occupied and unoccupied states, the p-orbital distribution of the O_{3c} atom is clearly illustrated.

After the AIMD simulations, the length of N-N and N-O bonds changes from a uniform value of 1.15 Å to 1.14 Å and 1.22 Å, respectively. The distance of the N_2O molecule from the surface is increased from 2.09 Å in the initial configurations to 2.44 Å in the final configurations. The linear geometry of the N_2O molecule is also slightly tilted with an angle of 155.81°. This tilted configuration of the N_2O affects the straight Ti–N bonds on the top surface and causes the lattice distortions. This may increase the total energy and could be one of the reasons for the low stability of the final configurations. Hence, it is proved that an N_2O molecule with a linear configuration is more preferable for adsorption. Our STM and AIMD simulations clearly emphasize that N_2O is adsorbed on the TiO₂ surface in a linear configuration only.

The thermal and dynamic stability of N_2O adsorbed on the rutile TiO_2 (110) surface is further studied by *Ab initio* molecular dynamics calculations as in the previous cases shown in Fig. 15. From the plot (Fig. 15(a)), it is found that the adsorbed system is thermodynamically stable throughout the MD steps. However, as seen in Fig. 15(b), the starting

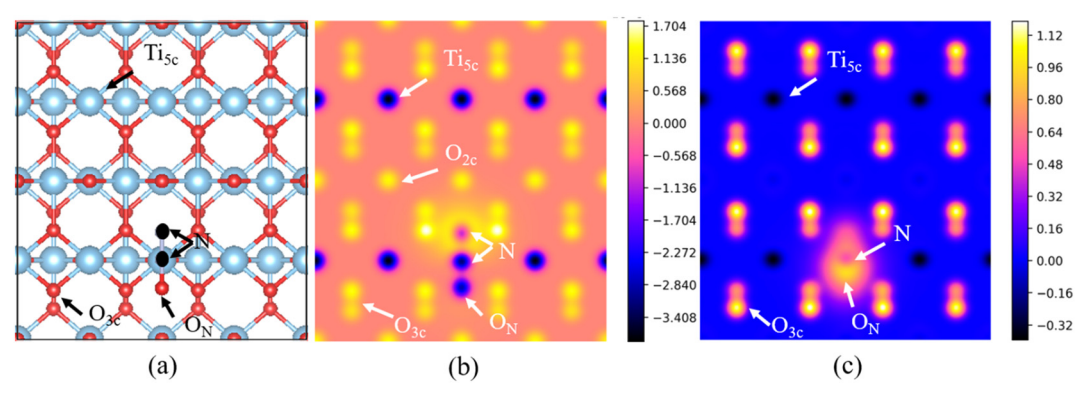


Fig. 14 (a) Top view of the calculated geometrical structure for N₂O adsorbed on the Ti_{5c} site of the rutile TiO₂ (110) surface, where Ti, O, and N atoms are shown in blue, red, and black, respectively. (b) Simulated STM image in the occupied state with V = -2.0 V. (c) Simulated STM image in unoccupied states with V = 2.0 V.

configurations have a lower energy compared to the final configurations. Fig. 15(c) shows the initial and final adsorbed configurations of N2O.

3.5. Outcome of the results

To propose a practical methodology for experimentally reducing the harmful NO_x pollutant, it is very important to understand the interaction of the gas pollutant with the photocatalytic surface. The process of pollution reduction on photocatalytic surfaces is highly dependent on active adsorption sites and the charge transport mechanism. Also, in order to compare with real case scenarios, experimentally it is difficult to explore the intricate features and the influence of NO_x on the electronic structure of photocatalysts. From our DFTbased calculations, we provide complete supportive guidelines for the analysis of NO_x adsorption on the TiO₂ photocatalyst surface. From the adsorption energetics, we propose the most favourable adsorption site of the different NO_x molecules on the TiO2 surface. From the state-of-the-art analysis, we had shown the complete description of charge transport mechanisms such as the acceptor or donor characteristics of the NO_x molecule. We explored the type of adsorption behaviour such as the chemisorption/physisorption of the pollutant on the TiO₂ surfaces. This analysis gives the key information for synthesizing the surface photocatalyst for achieving the

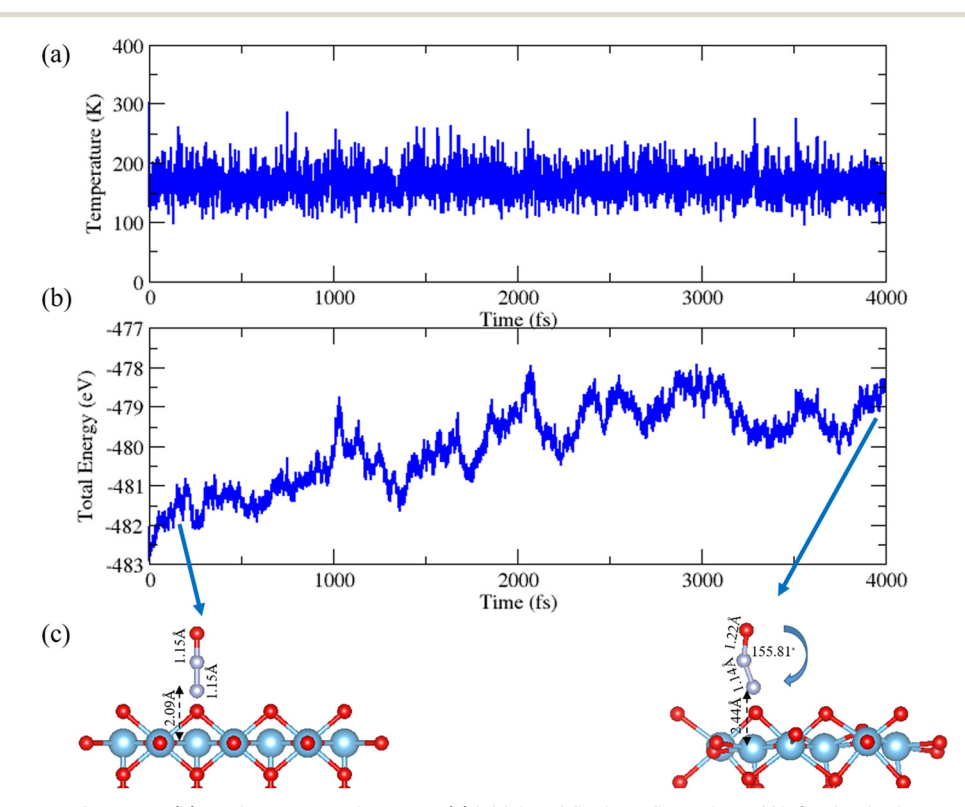


Fig. 15 (a) Temperature vs. time step, (b) total energy vs. time step, (c) initial and final configuration of N₂O adsorbed on rutile TiO₂.

selectivity and sensitivity of the NO_x gases. For the first time, we attempted to study the surface morphology of NOxadsorbed TiO2 surfaces by STM simulation. The adsorption configuration and the orbital distribution of the gases adsorbed on the TiO2 surface are analysed. This information will directly help researchers. One can compare their experimental STM images with simulated STM images, to study the surface morphology and surface chemistry of gas adsorption on the TiO2 surface. Finally, researchers needed to set up for NOx sensing and reduction with photocatalysts based on TiO2 surfaces at room temperature. Hence, our AIMD analysis at 300 K provides suggestions regarding the thermal and dynamic stability of the three different NOx adsorbed on the TiO₂ surfaces. From the AIMD results, the most stable geometry and the bond lengths and angles of NOx molecules are obtained. Hence, based on the above information, our results provide the pathway to experimentally investigate the NO_x sensitivity and selectivity mechanism for the application of reducing environmental pollutants.

4. Conclusion

Nitrogen oxides such as NO, NO2, and N2O are the major environmental pollutants arising from vehicle exhausts. In this work, we analyzed the interaction of NO_x molecules on pure and defective rutile TiO2 (110) surfaces using density functional theory. By calculating the adsorption energy in the pure rutile TiO₂ (110) surface, we found that among the various adsorption configurations, NO with N down on the O2c site, NO2 with O down on the Ti_{5c} site, and N₂O with N down on the Ti_{5c} site are found to be the most favorable adsorption configurations. The flow of charge between the molecules and the surface of these adsorbed configurations is explained with the help of electronic structures and charge-density plots. The surface morphology of the adsorbed molecules in their stable geometrical arrangements on rutile TiO2 (110) surfaces is studied by bias-dependent STM image simulation, which can be directly compared with experimental studies. The AIMD simulations are carried out to study the thermal and dynamic stability of the NO_x adsorbed on the TiO2 surfaces.

It is understood that NO-adsorbed ${\rm TiO_2}$ shows the nonnegligible covalent interaction between N-O_(Ti) atoms. The ${\rm TiO_2}$ surface gains electrons from the NO molecule, whereas the NO molecule gains a net charge of +0.20e from the surface. From AIMD, the adsorbed configurations are thermally stable for the entire MD simulation range (1 to 4000 fs at around 300 K). The most dynamically stable configurations are found in the middle of the MD step at 2081 fs, where the NO bond elongates from 1.15 Å to 1.21 Å with a small tilting in the bond with the surface.

For the case of NO_2 -adsorbed TiO_2 , a highly localized energy level of the NO_2 molecule falls on the Fermi level, which indicates the possible instability of the NO_2 molecule on the surface. An ionic bond between the $O_{(N)}$ - $Ti_{(5c)}$ atom is seen with a net transfer of negative charge (-0.34e) from the surface to the molecule; here, NO_2 gains a negative charge of -0.34e from the

 ${
m TiO_2}$ surface. Interestingly, for the ${
m NO_2}$ molecule, the initial adsorbed configuration with symmetric O–N–O bond lengths and equal Ti–O(N) bond distances is more preferable. The final configuration is unstable with non-symmetric O–N–O bond distances (1.41 Å, and 1.16 Å), with one of the ${
m O_{(N)}}$ atoms moving closer to the Ti atom on the top of the surface.

Interestingly, among the three nitrogen oxide molecules studied in this present work, the N_2O molecule has the least interaction with the surface with only the bottom N atom of N_2O binding with the surface. There is a weak chemical bond between the N atom of N_2O and with the Ti_{5c} atom, with very little charge transfer between the molecule and the surface. In the case of adsorption, there is an alteration in the bond length after the MD steps along with the tilting of the bonds in N_2O . These configurations of the N_2O affect the straight Ti-N bonds on the top surface and cause local distortions on the TiO_2 surface which may further increase the total energy. This could be one of the reasons for the lower stability of the final N_2O configurations.

Our DFT analysis can help to understand the surface chemistry of NO_x -adsorbed TiO_2 surfaces, and motivate further experimental studies for the reduction of harmful NO_x pollutants.

Data availability

The research data will be available upon request.

Author contributions

S. Muthukrishnan: conceptualization, investigation, data curation, formal analysis, performing the analysis, collecting the data, and writing the original draft. R. Vidya: conceptualization, investigation, data curation, formal analysis, performing the analysis, collecting the data, and writing the original draft. Anja Olafsen Sjåstad: conceptualization, investigation, and formal analysis.

Conflicts of interest

The authors declare that they don't have any conflict of interest.

Acknowledgements

The authors are grateful to the University of Oslo, Norway for providing the financial grant through the Indo-Norway project titled "Oxide Surfaces for Nitrous Oxide Abatement" (CIR/60/INDO-NORWAY/2019). The authors are also thankful to the Norwegian supercomputer facilities (Project No: NN2875K) for computing time.

References

 O. Badr and S. D. Probert, Environmental impacts of atmospheric nitrous oxide, *Appl. Energy*, 1993, 44(3), 197–231, DOI: 10.1016/0306-2619(93)90018-K.

- 2 C. Baukel, et al., Everything you need to know about NOx: controling and minimizing the pollutant emissions is crictical for meeting air quality regulations, Met. Finish., 2005, 103(11), 18-24.
- 3 T. Boningari and P. G. Smirniotis, Impact of nitrogen oxides on the environment and human health: Mn-based materials for the NOx abatement, Curr. Opin. Chem. Eng., 2016, 13, 133-141, DOI: 10.1016/j.coche.2016.09.004.
- 4 Z. Liu, J. Li, S. I. Woo and H. Hu, Density Functional Theory Studies of NO and NO2 Adsorption on Al2O3 Supported SnO2 Cluster, Catal. Lett., 2013, 143(9), 912-918, DOI: 10.1007/s10562-013-1072-9.
- 5 Y. Jin, C. Sun and S. Su, Experimental and theoretical study of the oxidation of ventilation air methane over Fe2O3 and CuO, Phys. Chem. Chem. Phys., 2015, 17(25), 16277-16284, DOI: 10.1039/c5cp00761e.
- 6 M. A. Gómez-García, V. Pitchon and A. Kiennemann, Pollution by nitrogen oxides: An approach to NOx abatement using sorbing catalytic materials, Environ. 2005, 31(3), 445-467, DOI: 10.1016/j.envint.2004.09.006.
- 7 Z. Yang, T. K. Woo and K. Hermansson, Adsorption of NO on unreduced and reduced CeO2 surfaces: A plane-wave DFT study, Surf. Sci., 2006, 600(22), 4953-4960, DOI: 10.1016/j. susc.2006.08.018.
- 8 Y. H. Lu and H. T. Chen, Computational investigation of NO2 adsorption and reduction on ceria and M-doped CeO2 (111) (M = Mn, Fe) surfaces, *I. Phys. Chem. C*, 2014, **118**(19), 10043-10052, DOI: 10.1021/jp412417e.
- 9 S. N. Hong, et al., Ab initio thermodynamic study of the SnO 2 (110) surface in an O 2 and NO environment: A fundamental understanding of the gas sensing mechanism for NO and NO 2, Phys. Chem. Chem. Phys., 2016, 18(46), 31566-31578, DOI: 10.1039/c6cp05433a.
- 10 F. Cao, et al., Density functional study of adsorption properties of NO and NH 3 over CuO/γ-Al 2 O 3 catalyst, Appl. Surf. Sci., 2012, 261(2), 659-664, DOI: 10.1016/j.apsusc.2012.08.077.
- 11 J. Jin, N. Sun, W. Hu, H. Yuan, H. Wang and P. Hu, Insight into Room-Temperature Catalytic Oxidation of Nitric oxide by Cr2O3: A DFT Study, ACS Catal., 2018, 8(6), 5415-5424, DOI: 10.1021/acscatal.8b00081
- 12 J. S. Dalton, P. A. Janes, N. G. Jones, J. A. Nicholson, K. R. Hallam and G. C. Allen, Photocatalytic oxidation of NOx gases using TiO2: A surface spectroscopic approach, Environ. Pollut., 2002, 120(2), 415-422, DOI: 10.1016/S0269-7491(02)00107-0.
- 13 S. Fukahori, H. Ichiura, T. Kitaoka and H. Tanaka, Photocatalytic Decomposition of Bisphenol A in Water Using Composite TiO2-Zeolite Sheets Prepared by a Papermaking Technique, Environ. Sci. Technol., 2003, 37(5), 1048-1051.
- 14 J. Zhang, Y. Wu, M. Xing, S. A. K. Leghari and S. Sajjad, Development of modified N doped TiO2 photocatalyst with metals, nonmetals and metal oxides, Energy Environ. Sci., 2010, 3(6), 715–726, DOI: 10.1039/b927575d.
- 15 S. Muthukrishnan, R. Vidva and A. Olafsen, Band gap engineering of anatase TiO 2 by ambipolar doping: A first principles study, Mater. Chem. Phys., 2023, 299, 127467, DOI: 10.1016/j.matchemphys.2023.127467.

- 16 M. Ramamoorthy and D. Vanderbilt, First-principles calculations of the energetics of stoichiometric Ti02 surfaces, Phys. Rev. B, 1994, 49, 16721-16727.
- 17 C. Lun Pang, R. Lindsay and G. Thornton, Chemical reactions on rutile TiO2(110), Chem. Soc. Rev., 2008, 37(10), 2328-2353, DOI: 10.1039/b719085a.
- 18 N. Cadmen, J. Bustamante, R. Rivera, F. J. Torres and J. Ontaneda, Dopamine Adsorption on Rutile TiO 2 (110): Geometry, Thermodynamics, and Core-Level Shifts from First Principles, ACS Omega, 2022, 7(5), 4185-4193, DOI: 10.1021/acsomega.1c05784.
- 19 D. C. Sorescu, C. N. Rusu and J. T. Yates, Adsorption of NO on the TiO2(110) Surface: An Experimental and Theoretical Study, I. Phys. Chem. B, 2000, 104(18), 4408-4417, DOI: 10.1021/jp993694a.
- 20 K. Erme, J. Raud and I. Jõgi, Adsorption of Nitrogen Oxides on TiO2 Surface as a Function of NO2 and N2O5 Fraction in the Gas Phase, Langmuir, 2018, 34(22), 6338-6345, DOI: 10.1021/acs.langmuir.7b03864.
- Wanbayor, P. Deák, T. Frauenheim Ruangpornvisuti, First-principles investigation of adsorption of N 2O on the anatase TiO 2 (1 0 1) and the CO preadsorbed TiO 2 surfaces, Comput. Mater. Sci., 2012, 58, 24-30, DOI: 10.1016/j.commatsci.2012.01.015.
- 22 Y. Y. Yu, U. Diebold and X. Q. Gong, NO adsorption and diffusion on hydroxylated rutile TiO2(110), Phys. Chem. Chem. Phys., 2015, 17(40), 26594-26598, DOI: 10.1039/ c5cp04584c.
- 23 A. Abbasi and J. Jahanbin Sardroodi, N-doped TiO2 anatase nanoparticles as a highly sensitive gas sensor for NO2 detection: Insights from DFT computations, Environ. Sci.: Nano, 2016, 3(5), 1153-1164, DOI: 10.1039/c6en00159a.
- 24 S. Marutheeswaran, S. B. Mishra, S. C. Roy and B. R. K. Nanda, Mechanistic Understanding of NO2 Dissociation on a Rutile TiO2 (110) Surface: An Electronic Structure Study, J. Phys. Chem. C, 2020, 124(16), 8786-8794, DOI: 10.1021/acs. ipcc.0c00525.
- 25 L. Mino, M. Cazzaniga, F. Moriggi and M. Ceotto, Elucidating NOx Surface Chemistry at the Anatase (101) Surface in TiO2 Nanoparticles, J. Phys. Chem. C, 2023, 127(1), 437-449, DOI: 10.1021/acs.jpcc.2c07489.
- 26 H. Li, Y. Guo and J. Robertson, Calculation of TiO2 Surface and Subsurface Oxygen Vacancy by Screened Exchange Functional, J. Phys. Chem. C, 2015, 119(32), 18160-18166.
- T. Pabisiak and A. Kiejna, Energytics of oxygen vacancies at rutile TiO2 (110) surface, Solid State Commun., 2007, 144, 324-328.
- 28 G. Teobaldi, W. A. Hofer, O. Bikondoa, C. L. Pang, G. Cabailh and G. Thornton, Modelling STM images of TiO2(1 1 0) from first-principles: Defects, water adsorption and dissociation products, Chem. Phys. Lett., 2007, 437(1-3), 73-78, DOI: 10.1016/j.cplett.2007.01.068.
- 29 G. Kresse and J. Furthmüller, Efficient iterative schemes for ab initio total-energy calculations using a plane-wave basis set, Phys. Rev. B:Condens. Matter Mater. Phys., 1996, 54(16), 11169-11186, DOI: 10.1103/PhysRevB.54.11169.

- 30 G. Kresse and J. Furthmüller, Efficiency of ab-initio total energy calculations for metals and semiconductors using a plane-wave basis set, *Comput. Mater. Sci.*, 1996, **6**(1), 15–50, DOI: **10.1016/0927-0256(96)00008-0**.
- 31 J. P. Perdew, K. Burke and M. Ernzerhof, Generalized gradient approximation made simple, *Phys. Rev. Lett.*, 1996, 77(18), 3865–3868, DOI: 10.1103/PhysRevLett.77.3865.
- 32 D. Joubert, From ultrasoft pseudopotentials to the projector augmented-wave method, *Phys. Rev. B:Condens. Matter Mater. Phys.*, 1999, **59**(3), 1758–1775, DOI: **10.1103/PhysRevB.59.1758**.
- 33 T. Matsushima, *et al.*, Inclined N 2 desorption in N 2 O decomposition on Rh(1 1 0), *Appl. Surf. Sci.*, 2005, **244**, 141–144, DOI: **10.1016/j.apsusc.2004.09.132**.
- 34 E. Sanville, Improved grid-based algorithm for Bader charge allocation, *J. Comput. Chem.*, 2007, **28**, 899–908.
- 35 S. Grimme, J. Antony, S. Ehrlich and H. Krieg, A Consistent and Accurate Ab Initio Parametrization of Density Functional Dispersion Correction (DFT-D) for the 94 Elements H-Pu, *J. Chem. Phys.*, 2010, 132(15), 154104.
- 36 K. Momma and F. Izumi, VESTA 3 for three-dimensional visualization of crystal, volumetric and morphology data, *J. Appl. Crystallogr.*, 2011, 44(6), 1272–1276, DOI: 10.1107/S0021889811038970.
- 37 A. Kokalj, XCrySDen-a new program for displaying crystalline structures and electron densities, *J. Mol. Graphics Modell.*, 1999, 17(3–4), 176–179, DOI: 10.1016/S1093-3263(99)00028-5.
- 38 V. Wang, N. Xu, J. C. Liu, G. Tang and W. T. Geng, VASPKIT: A user-friendly interface facilitating high-throughput computing and analysis using VASP code, *Comput. Phys. Commun.*, 2021, 267, 108033, DOI: 10.1016/j.cpc.2021.108033.
- 39 S. Maintz, V. L. Deringer, A. L. Tchougréeff and R. Dronskowski, LOBSTER: A tool to extract chemical bonding from plane-wave based DFT, *J. Comput. Chem.*, 2016, 37(11), 1030–1035, DOI: 10.1002/jcc.24300.
- 40 G. Kresse and J. Hafner, Ab initio molecular dynamics for liquid metals, *Phys. Rev. B: Condens. Matter Mater. Phys.*, 1993, 47(1), 558–561, DOI: 10.1103/PhysRevB.47.558.
- 41 G. Kresse and J. Hafner, Ab initio molecular-dynamics simulation of the liquid-metalamorphous- semiconductor transition in germanium, *Phys. Rev. B: Condens. Matter Mater. Phys.*, 1994, 49(20), 14251–14269, DOI: 10.1103/PhysRevB.49.14251.
- 42 W. Wei, *et al.*, Density Functional Characterization of the Electronic Structures and Band Bending of Rutile RuO2/TiO2(110) Heterostructures, *J. Phys. Chem. C*, 2015, **119**(22), 12394–12399, DOI: **10.1021/acs.jpcc.5b01884**.

- 43 A. Rønnau, A Closer Look at the TiO₂(110) Surface with STM, PhD thesis, University of Aarhus, Denmark, 2003, [Online]. Available: https://www.phys.au.dk/fileadmin/site_files/publikationer/phd/Anders_Ronnau.pdf.
- 44 S. J. Tan and B. Wang, Active Sites for Adsorption and Reaction of Molecules on Rutile TiO2(110) and Anatase TiO2(001) Surfaces, *Chin. J. Chem. Phys.*, 2015, **28**(4), 383–395, DOI: **10.1063/1674-0068/28/cjcp1506129**.
- 45 B. J. Morgan and G. W. Watson, A DFT+U description of oxygen vacancies at the TiO2 rutile (110) surface, *Surf. Sci.*, 2007, 601(21), 5034–5041, DOI: 10.1016/j.susc.2007.08.025.
- 46 J. Tersoff and D. R. Hamann, Theory of the scanning tunneling microscope, *Phys. Rev. B: Condens. Matter Mater. Phys.*, 1985, 31(2), 805–813, DOI: 10.1103/PhysRevB.31.805.
- 47 A. Mugarza, C. Krull, R. Robles, S. Stepanow, G. Ceballos and P. Gambardella, Spin coupling and relaxation inside molecule-metal contacts, *Nat. Commun.*, 2011, 2(1), DOI: 10.1038/ncomms1497.
- 48 A. D. Gottlieb and L. Wesoloski, Bardeen's tunnelling theory as applied to scanning tunnelling microscopy: A technical guide to the traditional interpretation, *Nanotechnology*, 2006, 17(8), DOI: 10.1088/0957-4484/17/8/R01.
- 49 T. Minato, *et al.*, The electronic structure of oxygen atom vacancy and hydroxyl impurity defects on titanium dioxide (110) surface, *J. Chem. Phys.*, 2009, **130**(12), DOI: **10.1063**/**1.3082408**.
- 50 K. Choudhary, *et al.*, Computational scanning tunneling microscope image database, *Sci. Data*, 2021, 1–9, DOI: 10.1038/s41597-021-00824-y.
- 51 C. Di Valentin, Scanning tunneling microscopy image simulation of the rutile (110) Ti O2 surface with hybrid functionals and the localized basis set approach, *J. Chem. Phys.*, 2007, 127(15), DOI: 10.1063/1.2790430.
- 52 W. B. Maddox, D. P. Acharya, G. J. Leong, P. Sutter and C. V. Ciobanu, Bias-Dependent Scanning Tunneling Microscopy Signature of Bridging-Oxygen Vacancies on Rutile TiO2(110), *ACS Omega*, 2018, 3(6), 6540–6545, DOI: 10.1021/acsomega.8b01056.
- 53 V. L. Deringer, A. L. Tchougr and R. Dronskowski, Crystal Orbital Hamilton Population (COHP) Analysis As Projected from Plane-Wave Basis Sets, *Sets J. Phys. Chem. A*, 2011, 115(21), 5461–5466, DOI: 10.1021/jp202489s.
- 54 M. Setvin, *et al.*, Identification of adsorbed molecules via STM tip manipulation: CO, H2O, and O2 on TiO2 anatase (101), *Phys. Chem. Chem. Phys.*, 2014, **16**(39), 21524–21530, DOI: **10.1039/c4cp03212h**.